Article

Porous Fe-Porphyrin as an Efficient Adsorbent for the Removal of Ciprofloxacin from Water

Shabnam Mehraban Khaledi, Masoumeh Taherimehr,* and Seyed Karim Hassaninejad-Darzi

Cite This: ACS Omega 2024, 9, 15950−15958

Read Online

ACCESS | Metrics & More | Article Recommendations | SI Supporting Information

ABSTRACT: Antibiotics are widely used in medicine, but they are not fully metabolized in the body and can end up in wastewater. Conventional wastewater treatment methods fail to completely remove antibiotic residues, which can then enter rivers and streams. Adsorption is a promising technique for removing antibiotics from wastewater, even at low concentrations. The successful one-pot synthesis of an adsorbent, iron-containing porphyrin-based porous organic polymer (Fe-POP), was achieved through the reaction of pyrrole groups and terephthalaldehyde in the presence of $FeCl_3$. Characterized by a substantial BET surface area of 597 m^2 g^{-1}, Fe-POP was systematically investigated for its adsorption potential in the removal of the antibiotic Ciprofloxacin (CIP) from aqueous solutions. By systematic variation of key parameters, including pH, adsorbent loading, and CIP concentration, the adsorption conditions were optimized. Under the optimal conditions at pH = 3, CIP concentration of 5 ppm, and 25 mg of Fe-POP, the maximum adsorption capacity reached an impressive 263 mg g^{-1}. The robust adsorption behavior was elucidated through the fitting of experimental data to the Langmuir adsorption isotherm ($R^2 = 0.962$) and the pseudo-second-order kinetic model ($R^2 = 0.999$) with lower error values. These models suggested that the adsorption process predominantly involved chemical interactions between CIP molecules and the Fe-POP surface. Fe-POP exhibited a robust structure with a high adsorption capacity, showcasing its efficacy in removing CIP contaminants from water. Therefore, Fe-POP can be considered a valuable adsorbent for water treatment applications, specifically for antibiotic removal.
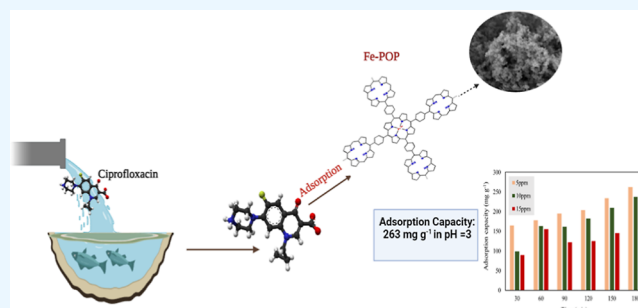
1. INTRODUCTION

There is an increasing focus on minimizing environmental impact, advancing sustainability, and promoting the well-being of both current and future generations.[1] Scientists are exploring diverse approaches to address global challenges related to sustainability.[2,3] In recent decades, escalating water pollution, driven by population growth and human activities, has emerged as a major concern for human health. The release of hazardous pollutants into water systems is linked to issues such as bacterial resistance and a rise in hormonal and genetic diseases.[4] These hazardous pollutants include pesticides, aromatic compounds, dyes, and antibiotics, which have been found in groundwater.[5] Antibiotics are a group of organic substances that work as opposed to a wide range of microbial strains.[6,7] However, their excessive use and release into groundwater sources increase the resistance of Gram-negative and Gram-positive bacteria in the water, and as a result, these bacteria enter the food chain and cause disease.[8] Ciprofloxacin (CIP), the most commonly prescribed fluoroquinolone antibiotic,[9] has been observed in the wastewater of hospitals, pharmaceutical industries, and groundwater.[10] There have been numerous treatment methods for the elimination of CIP from wastewater, such as membrane technology,[11] ozonation,[12] photocatalytic degradation,[13] electrochemical degradation,[14] and adsorption.[15] Adsorption, which

has suitable features for antibiotic removal from water like low cost, high performance, and flexibility, is known as a promising and popular method for removing CIP from wastewater.[16,17] Materials like activated carbon,[18] semiconductor materials,[19] and porous materials, including zeolites,[20] silicates,[21] metal−organic frameworks (MOFs),[22] and porous organic polymers (POPs),[23] have been used for removing CIP from water via the adsorption method. A study on the adsorptive removal of ciprofloxacin CIP from the aqueous medium used the magnetic guar gum-grafted graphene oxide nanocomposite (mGG/GO NC), which showed a high adsorption capacity for the removal of CIP of 222.22 mg g^{-1} at pH 7.0 and 25 °C.[24]
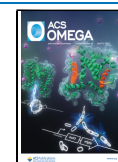
Porous organic polymers represent a new class of multidimensional porous network materials, characterized by robust covalent linkages between diverse organic building blocks featuring various geometries and topologies. This class of

Scheme 1. Preparation of Fe-POP Synthesize Steps
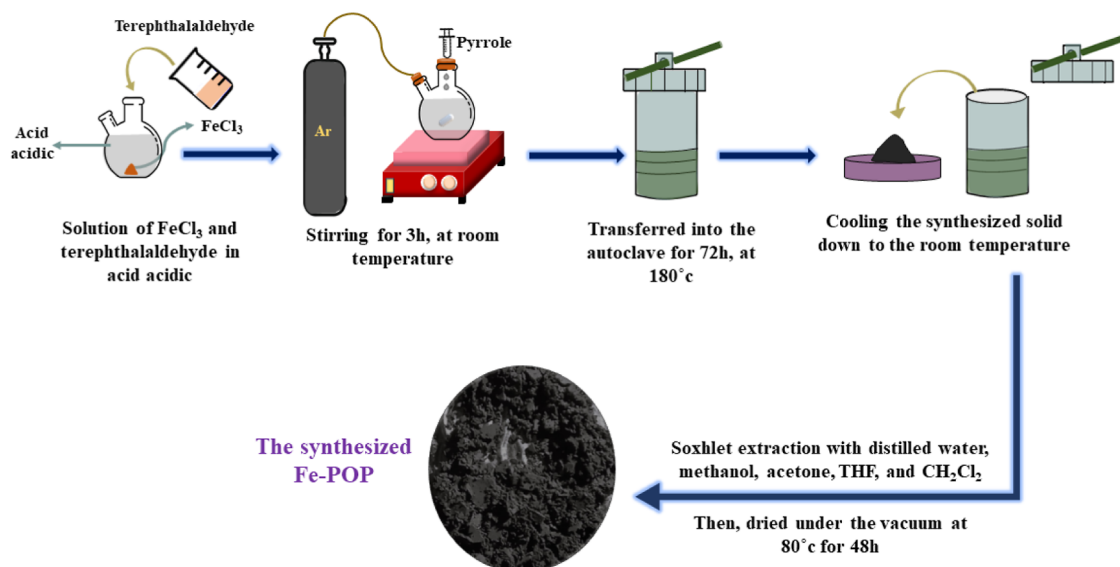

materials has recently emerged as a prominent area of investigation within the field of porous materials. Leveraging their inherent advantages, such as lightweight composition, exceptional porosity, robust stability, and the ability to predesign and tune structures and functionalities, POPs have received increasing attention and research interest.[25] These unique attributes position them as promising candidates for diverse applications, including but not limited to gas storage and separation, heterogeneous catalysis, photoelectric synthesis, biosensing, and adsorption.[26−30]

Porphyrin-based porous organic polymers, or porous porphyrins, abbreviated as POPs, are a class of materials that combine the advantages of porous organic polymers and porphyrins, including a large specific surface area and high porosity. In recent years, POPs have been increasingly studied and widely used in various fields such as photocatalysis,[31] electrocatalysis,[32] storage,[33] and adsorption.[34] The central metal ions and surrounding functional groups of porphyrins can be modified to meet the needs of different applications. Iron-containing adsorbents, such as MOFs,[35] chitosan,[36] zeolites,[37] and layered double hydroxides,[38] have been investigated in the adsorptive removal of antibiotics from water. For instance, a recent study reported the use of magnetic rod-like hydroxyapatite and MIL-101(Fe) MOF nanocomposite for the removal of TC and CIP antibiotics from water with removal efficiencies of 95 and 93%, respectively.[39] Another study reported the use of FeCl$_3$-modified sawdust for the removal of TC from water. The adsorption capacity of FeCl$_3$-modified sawdust was found to be higher than that of raw sawdust. The presence of carbon, oxygen, and iron on the surface of the raw sawdust allowed for more functional groups, such as hydroxyl, carboxyl, carboxylate, and ferric, to be available due to the deposition of FeCl$_3$ on the surface of the sorbent material.[40] As mentioned, Fe-based adsorbents have shown remarkable potential for the removal of antibiotics from water. To the best of our knowledge, no reports have been published on the use of iron-containing porphyrin-based porous organic polymers for adsorbing antibiotics such as CIP, despite their potential as an effective adsorbent.

In this study, a porous organic polymer incorporating iron(III) centers, referred to as Fe-POP, is synthesized, and its potential is explored as an adsorbent for removing CIP from water. Fe-POP is synthesized by a facile one-pot bottom-up approach to porphyrin chemistry through an extended aromatic substitution reaction between pyrrole and aromatic dialdehydes in the presence of a small amount of Fe(III). This method is advantageous because it is simple and efficient.[41] We systematically investigated the optimal conditions for CIP adsorption by varying various parameters, and additionally, we conducted a detailed study of the kinetics of the adsorption process.

2. MATERIALS AND EXPERIMENTS

2.1. Materials and Characterization. All chemicals used in the experiments are of analytical-grade purity and are not subject to further purification.

Pyrrole (C_4H_5N), terephthalaldehyde ($C_8H_6O_2$), and iron-(III) chloride (FeCl$_3$) were purchased from the pharmaceutical company Merck, and CIP ($C_{17}H_{18}FN_3O_3$) was purchased from the pharmaceutical company Farabi.

The characteristics of the Fe-POP chemical structure and conformation were determined by Fourier transform infrared (FT-IR) spectroscopy in the 500−4000 cm^{-1} range at room temperature on a Thermo Avatar. The morphology of samples was characterized by scanning electron microscopy (SEM) on SEM VEGA3 operated at 20 kV after sputter-coating with gold. Nitrogen adsorption/desorption isotherm analyses were performed at 77 K on a MICROMERITICS Asap2020. The ultraviolet spectrum (UV) was measured by a UNICO, UV-2100 spectrophotometer. The EDS spectrum was measured by a ZISS SIGMA-3000.

2.2. Synthesis of the Iron-Containing Porphyrin-Based Porous Organic Polymer (Fe-POP). Fe-POP was synthesized following the reported procedure.[42] Scheme 1 illustrates the steps of Fe-POP's synthesis. A solution of iron(III) chloride (0.44 mmol) and terephthalaldehyde (0.05 g, 0.37 mmol) in acetic acid (15 mL) was prepared, followed by the slow addition of pyrrole (0.025 g, 0.37 mmol) under an Ar atmosphere and vigorous stirring at RT for 1 h. Then, the viscous dark brown solution was transferred to a Teflon-lined hydrothermal autoclave and kept at 180 °C for 72 h.

After the autoclave was cooled to room temperature, the dark brown solid was isolated from the reaction mixture, followed by
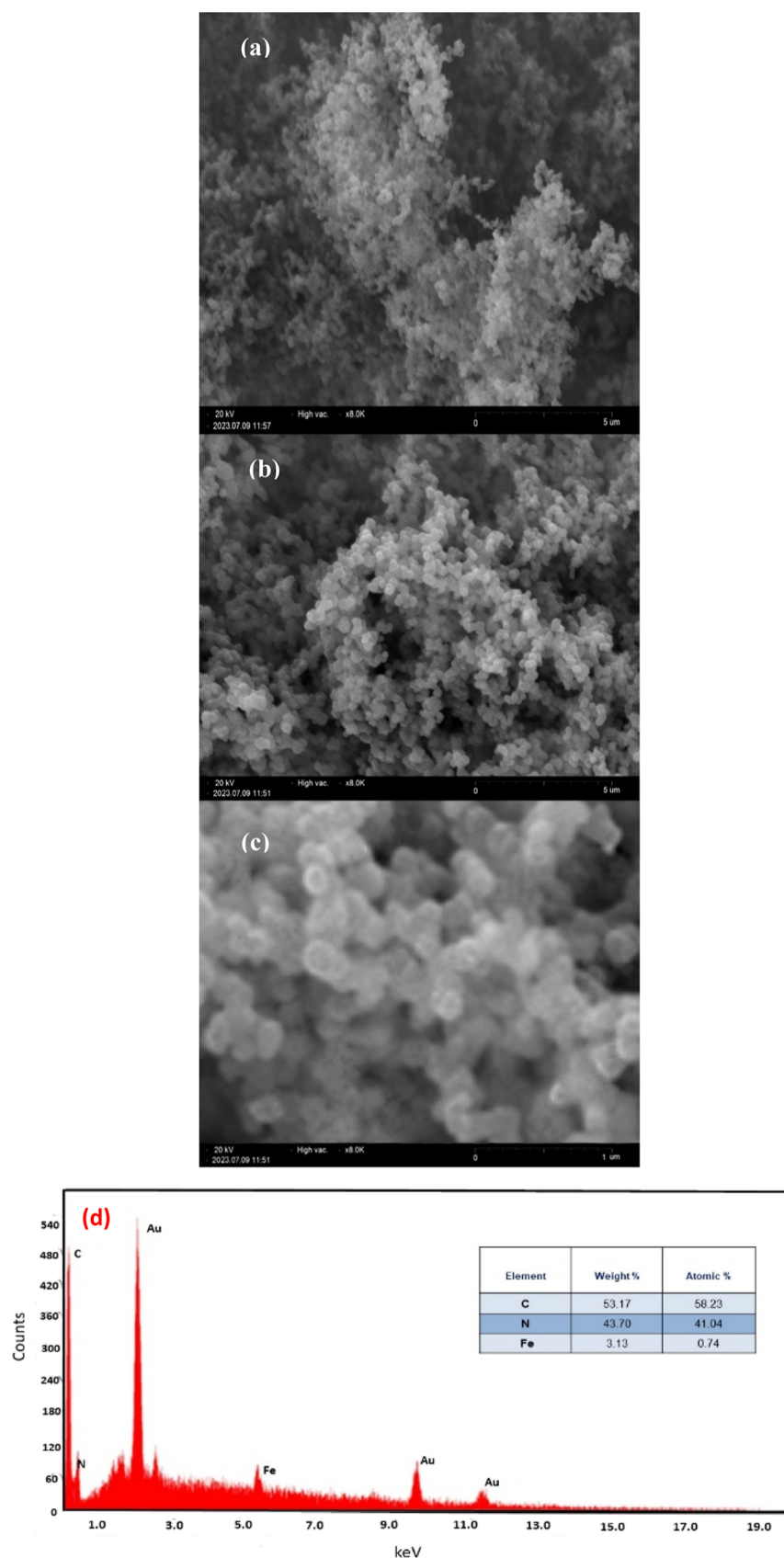
Figure 1. SEM image of the synthesized Fe-POP (a−c) and the EDS spectrum of the synthesized Fe-POP (d).

Soxhlet extraction with distilled water, methanol, acetone, THF, and CH_2Cl_2 sequentially. Then, the solid was dried under a vacuum at 80 °C for 48 h.

2.3. Adsorption Test. First, an aqueous stock solution of CIP was prepared by adding 20 mg of CIP to 200 mL of deionized water and stirring for 1 h at RT. 25 mg portion of the
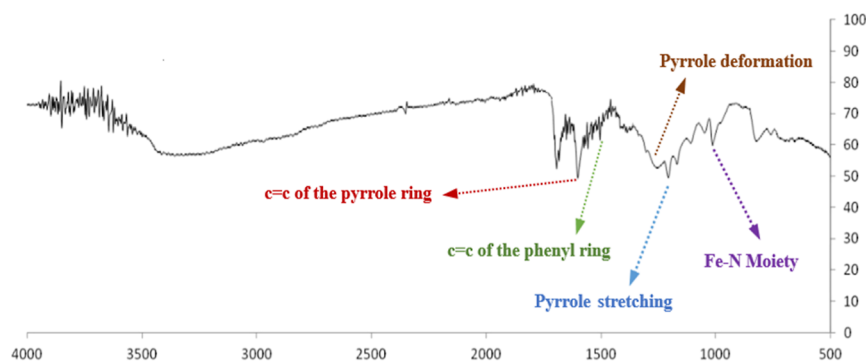
Figure 2. FT-IR spectrum of synthesized Fe-POP.

adsorbent was added to a 50 mL CIP solution (5 ppm) mixture and stirred at 450 rpm at RT for a certain time. After adsorption, the adsorbent was separated by centrifugation at 3000 rpm after 10 min. Then, the solutions were filtered over a 0.22 μm cellulose triacetate syringe filter, and the residual concentrations of CIP in the liquid phase were measured with a UV−vis spectrophotometer at a wavelength of 271 nm. The adsorption of CIP at various concentrations of the pollutant, adsorbent loading, and pH of the solution were investigated. Adsorption capacity was calculated by the following eq 1

$$Q_e = \frac{(C_0 - C_e) \times V}{W} \tag{1}$$

The initial concentration and equilibrium concentration of CIP are C_0 (mg L^{-1}) and C_e, respectively. The volume of the CIP solution is V (L), and the Fe-POP dosage is W (g).

2.4. Kinetic and Equilibrium Study. The adsorption isotherm of this study was investigated by fitting the experimental data with the Langmuir and Freundlich adsorption isotherm models in eqs 2 and 3, respectively. Three 50 mL CIP solutions at concentrations of 5, 10, and 15 ppm were prepared, and each solution was mixed with 25 mg of Fe-POP at pH 3.

$$\frac{C_e}{q_e} = \left(\frac{1}{q_{max} \times K_L}\right) + \frac{C_e}{q_{max}} \tag{2}$$

$$\log q_e = \log k_f + \left(\frac{1}{n}\right)\log c_e \tag{3}$$

The equilibrium concentration of CIP in solution is C_e (mg L^{-1}), the corresponding equilibrium adsorption capacity of CIP is q_e (mg L^{-1}), the saturated monolayer is q_{max} (mg g^{-1}), the Langmuir and Freundlich adsorption constants are K_L (L mg^{-1}) and K_f (mg$^{1-1/n}$ L$^{1/n}$ g^{-1}) respectively, and n is the adsorption intensity of CIP by Fe-POP at an equilibrium state.

The pseudo-first-order law and pseudo-second-order law in eqs 4 and 5, respectively, were applied to examine the adsorption kinetics. The test was conducted with 50 mL of CIP solution at a 5 ppm concentration and pH 3. The examination duration ranged from 30 to 120 min.

$$\ln(q_e - q_t) = \ln q_e - k_1 t \tag{4}$$

$$\frac{t}{q_t} = \frac{1}{q_e{}^2 k_2} + \frac{1}{q_e} t \tag{5}$$

The amounts of pollutant adsorbed at equilibrium time and specific time (min) are q_e and q_t (mg g^{-1}), respectively, in this equation. Also, K_1 (min^{-1}) and K_2 (g mg^{-1} min^{-1}) are the

constants of the pseudo-first-order and pseudo-second-order kinetic equations, respectively.

2.5. Error Analysis. In this study, we used error functions including sum square error (ERRSQ), hybrid functional error (HYBRID), and average relative error (ARE), as described in eqs 6, 7, and 5, respectively, to determine the best fitting models for adsorption data.[43] The quality of a model is better when the error values for a given isotherm or kinetic model are lower.[44]

$$\sum_{i=1}^{n} (q_{e,calc} - q_{e,exp})_i^2 \tag{6}$$

$$\frac{100}{p - n} \sum_{i=1}^{n} \left[\frac{(q_{e,i,calc} - q_{e,i,exp})^2}{q_{e,i,exp}}\right] \tag{7}$$

$$\frac{100}{n} \sum_{i=1}^{n} \left|\frac{(q_{e,i,calc} - q_{e,i,exp})}{q_{e,i,exp}}\right| \tag{8}$$

The subscripts "exp" and "calc" indicate the experimental and calculated values, respectively. The variable "n" represents the number of observations in the experimental data.

2.6. Point of Zero Charge of Fe-POP. In order to determine the point of zero charge of the absorbent, first a 0.01 M NaCl solution was prepared in a volume of 200 mL, and with hydrochloric acid and sodium hydroxide, the pH of each of the samples was adjusted to reach pH 3, 5, 7, 9, and 11. After that, 10 mg of Fe-POP was added to each of the beakers that had different pH levels, and the beakers were placed on a shaker at 150 rpm for 24 h. After 24 h, the final pH of these solutions was measured. The point of zero charge of the adsorbent is determined after obtaining the ΔpH diagram relative to the initial pH. ΔpH is calculated from eq 9

$$\Delta pH = pH_{initial} - pH_{final} \tag{9}$$

3. RESULTS AND DISCUSSION

3.1. Characterization of Fe-POP. Fe-POP was synthesized by reacting pyrrole and terephthalaldehyde in the presence of FeCl$_3$ to form polymers of porphyrin blocks according to the reported procedure.[42]

The Fe-POP solid-state ^{13}C NMR spectrum exhibited three resonance signals at δ: 129.3, 131.5, and 191.3, which could be assigned to the phenyl carbons, porphyrin macrocycles, and the terminal aldehyde groups, respectively (Figure S1). Figure 1a−c presents the morphology of Fe-POP as observed by scanning electron microscopy (SEM). The matrices exhibit spherical

particles with dimensions of approximately 60−100 nm, which undergo self-assembly to form larger, uniform spherical particles measuring around 250−750 nm. The elemental composition of Fe-POP, as determined by energy-dispersive X-ray (EDX) analysis, is depicted in Figure 1d. Carbon constitutes the majority, representing 58.23 atomic percentages, making it the most prevalent element. Nitrogen follows as the second dominant element, accounting for 41.04 atomic percentage. Despite the theoretical Fe weight percentage in a Fe-POP framework, where each porphyrin unit is occupied by an iron atom, being 7.9 wt %, the observed iron content is generally lower, aligning with prior reports. This finding underscores that a significant fraction of the porphyrin units lack iron, as demonstrated by the results.[42]

To characterize the material, the FT-IR spectrum was acquired (Figure 2). The band observed at 1601 cm^{-1} corresponds to the C=C stretching vibration in the pyrrole ring, while the band at 1267 cm^{-1} is attributed to pyrrole bending. Additionally, the band observed at 1211 cm^{-1} is associated with pyrrole stretching. The band located at 1504 cm^{-1} is indicative of C=C stretching vibrations in the phenyl rings. The presence of a band at 1014 cm^{-1} suggests the bonding of Fe(III) to the porphyrin units, forming Fe−N bonds.[41] Based on the FT-IR spectrum, it can be inferred that pyrrole and terephthalaldehyde groups have formed porphyrin units, which are repetitively connected by phenyl groups as bridges. Moreover, some of the porphyrin rings exhibit coordination with ferric ions (Scheme S1).

In Figure 3a, nitrogen sorption analysis at 77 K reveals that Fe-POP exhibits a microporous structure with pores smaller than 2
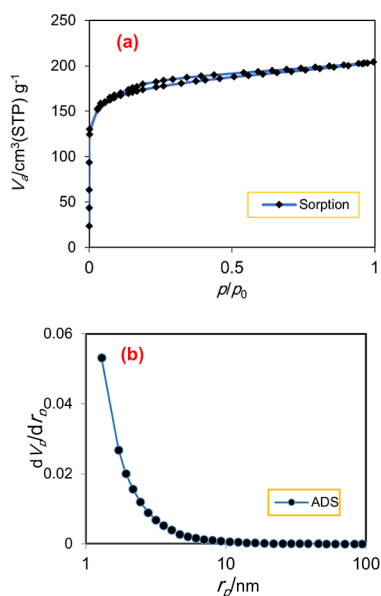

Figure 3. N$_2$ sorption isotherms (a) and pore size distribution of Fe-POP (b).

nm, as evidenced by the I-type isotherm. The Brunauer−Emmett−Teller (BJH) method was employed to assess the pore size distribution of Fe-POP. The pore size distribution diagram (Figure 3b) further substantiates the microporous nature of Fe-POP. The most prevalent pores exhibited a radius of 1.29 nm with an average pore size of 1.90 nm, placing them within the micropore range.[45,46]

3.2. Effect of Adsorbent Amount on CIP Adsorption.
To investigate how the amount of adsorbent affects the adsorption process, different amounts of adsorbent (12.5, 25, and 37.5 mg) were added to 50 mL of CIP solution with a concentration of 10 ppm at pH = 7. As Figure 4 illustrates, the
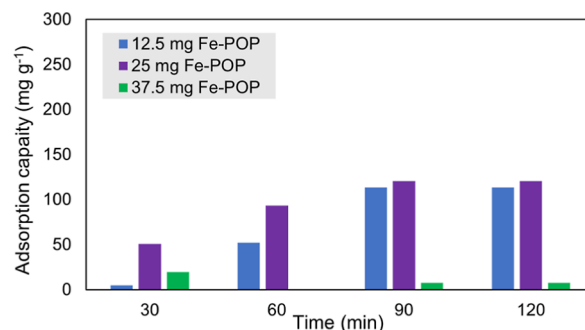

Figure 4. Effect of Fe-POP loading (12.5, 25, and 37.5 mg) on CIP adsorption in 50 mL of CIP at a concentration of 10 ppm and a pH of 7.

adsorption capacity of CIP increased slightly from 114 to 121 mg g^{-1} after 120 min when the amount of Fe-POP increased from 12.5 to 25 mg. This suggests that more CIP molecules were adsorbed from the solution by the increased surface area and active sites of Fe-POP. However, when the amount of Fe-POP increased further to 37.5 mg, the adsorption rate decreased to 7.8 mg g^{-1} after 120 min. This implies that adding more Fe-POP did not enhance the adsorption performance but rather had an adverse effect. A possible explanation for this phenomenon is that Fe-POP aggregated due to the π−π interactions between porphyrin layers at a high loading, which reduced the effective surface area and pore volume for adsorption. This created a mass transfer resistance or a diffusion barrier for CIP molecules to access the adsorption sites, which decreased the adsorption kinetics and equilibrium.

3.3. Effect of pH Medium on CIP Adsorption.
To evaluate the effect of pH on the adsorption rate, the adsorption experiments were conducted at pH values of 3, 7, and 11, by adding 25 mg of Fe-POP to the CIP solution with a concentration of 10 ppm. The results are illustrated in Figure 5. It was found that the highest adsorption capacity of CIP by Fe-POP was 203.5 mg g^{-1} after 180 min at pH = 3.

To understand the reason for this behavior, we determined the point of zero charge (PZC) of the adsorbent. The PZC value indicates the pH at which the adsorbent surface has no net
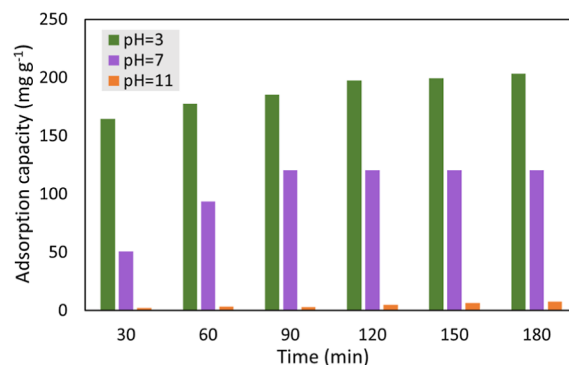

Figure 5. Effect of pH (3, 7, and 11) on CIP adsorption by Fe-POP at an Fe-POP loading of 25 mg and CIP concentration of 10 ppm.

charge, which affects its interaction with different ions and molecules in the solution.[47] The PZC value of Fe-POP was obtained by equilibrating it with solutions of varying initial pH values and measuring the change in pH (ΔpH) after adsorption. Figure 6 shows that the PZC value of Fe-POP is 6.3, meaning
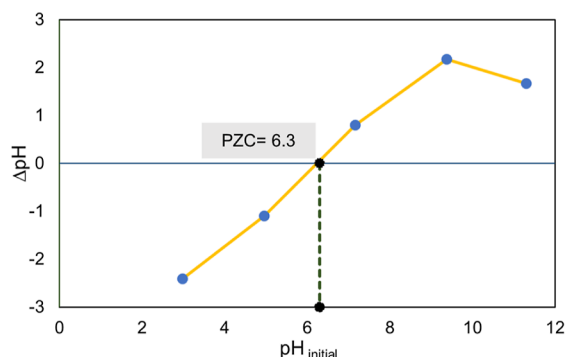

Figure 6. PZC of the synthesized Fe-POP.

that the adsorbent surface has equal amounts of H^+ ions and OH^- ions at this pH. Therefore, the adsorbent surface has neither a positive nor a negative charge at pH 6.3. Upon comparison of the PZC value with the adsorption results at different pH levels, it can be concluded that Fe-POP has a lower adsorption capacity for CIP at a basic pH, where the adsorbent surface acquires a negative charge. To elucidate this behavior, attention must be directed toward the ionic equilibrium of CIP. CIP has pK_{a1} = 6.09, pK_{a2} = 8.62, and pI = 7.14 (the isoelectric point, calculated as the average of pK_{a1} and pK_{a2}).[48] At a pH lower than 6.09, CIP primarily exists in its molecular form, while at a pH higher than 7, it predominantly exists in its anionic form. On the other hand, the adsorbent Fe-POP exists in a cationic form at pH levels below 6.3 (its PZC point) and transitions to an anionic state at pH levels exceeding 6.3. When considering both CIP and Fe-POP in a basic medium, both are in an anionic form, resulting in electrostatic repulsion that diminishes the adsorption. However, at an acidic pH, electrostatic repulsion is absent, allowing molecular interactions between CIP and Fe-POP. This includes the complexation of Fe with ciprofloxacin on the surface of Fe-POP[49,50] and $\pi-\pi$ interaction between the phenyl rings of Fe-POP and CIP, thereby enhancing the adsorption capacity of CIP on the surface of Fe-POP.[51]

3.4. Effect of CIP Concentration on Adsorption. To investigate the effect of pollutant concentration on the adsorption rate, the adsorption tests were performed at the optimum pH (3) with varying initial concentrations of CIP (5, 10, and 15 ppm) in the presence of 25 mg of Fe-POP. Figure 7 illustrates that the highest adsorption rate of CIP was achieved at 5 ppm, with an adsorption capacity of 263 mg g^{-1} which is significant compared to that of previously reported adsorbents (see Table 1). However, increasing the initial concentration of CIP from 5 to 15 ppm resulted in a decrease in the adsorption capacity, declining from 263 to 155 mg g^{-1} after 180 min. This suggests that a higher concentration of CIP in the solution can reduce the adsorption efficiency and effectiveness of Fe-POP. The competitive effect among CIP molecules for the available adsorption sites on Fe-POP might be the reason for this reduction in adsorption capacity and equilibrium.

3.5. Adsorption Isotherm and Models. The adsorption isotherm of CIP on Fe-POP was assessed by using the Langmuir and Freundlich models, and the experimental data were fitted to
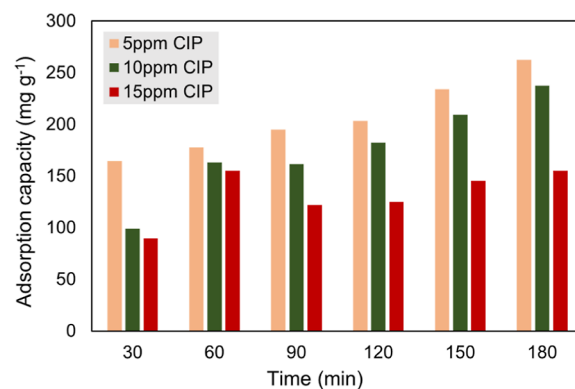

Figure 7. Effect of CIP concentration (5, 10, and 15.5 ppm) on the adsorption capacity at Fe-POP loading of 25 mg and pH of 3.

both models. The Langmuir model posits a homogeneous adsorbent surface with a finite number of identical adsorption sites. In this model, each site can bond only one adsorbate molecule, and there is no interaction between the adsorbed molecules. On the other hand, the Freundlich model suggests a heterogeneous adsorbent surface with a distribution of adsorption sites characterized by different sizes and energies. Each site in this model can adsorb more than one adsorbate molecule, and the adsorption process follows a power function.[56] The Langmuir isotherm model, known for its typical monolayer adsorption process, shows a high R^2 value (0.9626) and low ERRSQ (3.360), HYBRID (3.465), and ARE (5.575) compared to Freundlich isotherm parameters, which are shown in Table 2. These findings indicate that the experimental data on CIP adsorption fit better with the Langmuir isotherm and that CIP adsorption on Fe-POP follows the monolayer adsorption process.

3.6. Adsorption Kinetics and Modeling. The adsorption kinetics of CIP on Fe-POP were evaluated using both the first-order and second-order kinetic models. The adsorption kinetics within the time range of 30−120 min at an initial CIP concentration of 5 ppm are depicted in Figure 8. The kinetic parameters along with the R^2 and error values (i.e., ERSQ, HYBRID, and ARE) of the adsorption of CIP onto Fe-POP are shown in Table 3. The results of the pseudo-second-order kinetic model revealed that the value of R^2 is situated at 0.9991, indicating good fits for CIP adsorption on Fe-POP.

This model suggests that the adsorption process is predominantly governed by the chemical interaction between the CIP molecules and the surface of Fe-POP.

The adsorption capacity of Fe-POP is contingent on the number and strength of the chemical bonds formed during the adsorption process. As the number of available sites decreases, the rate of adsorption diminishes. This observation underscores the significance of chemical interactions in influencing the adsorption capacity of Fe-POP, highlighting its potential as an effective adsorbent for water treatment applications.[57,58]

4. CONCLUSIONS

The porphyrin-based porous polymer Fe-POP adsorbent was successfully prepared through a one-pot Friedel−Crafts reaction involving pyrrole groups and terephthalaldehyde in the presence of $FeCl_3$. The morphology, structure, and stability of as-prepared Fe-POP were studied by different characterization techniques, including SEM, EDX, FT-IR, BET, and solid-state ^{13}C NMR. Fe-POP exhibited a large specific surface area of 597 m^2 g^{-1}.

Table 1. Comparison of Previous Studies on Ciprofloxacin Adsorption from Water with Our Work

no.	adsorbent	composition	adsorption capacity $(mg\,g^{-1})$	references
1	Fe/Ni-MOF	iron and nickel ions as metal ion sources and 1,3,5-phthalic acid as the organic ligand	232	52
2	PAC@Fe$_3$O$_4$-MN	powdered activated carbon magnetized by iron(III) oxide	110	18
3	MCM-41-NH$_2$	amine-functionalized MCM-41	164	53
4	Chi-SiO$_2$/Fe$_3$O$_4$	chitosan-grafted SiO$_2$-Fe$_3$O$_4$	101	54
5	DDMGO	magnetic graphene oxide/diethylenetriaminepentaacetic acid	70−240	55
6	Fe-POP	Fe-porphyrin	263	this work

Table 2. Fitted Langmuir and Freundlich Isotherm Parameters and Error Values for the Adsorption of CIP

Langmuir					
q_{max}	K_l	R^2	ERRSQ	HYBRID	ARE
13.92	0.166	0.962	3.360	3.465	5.575
Freundlich					
n	K_f	R^2	ERRSQ	HYBRID	ARE
1.83	2.491	0.836	5.946	7.285	6.386
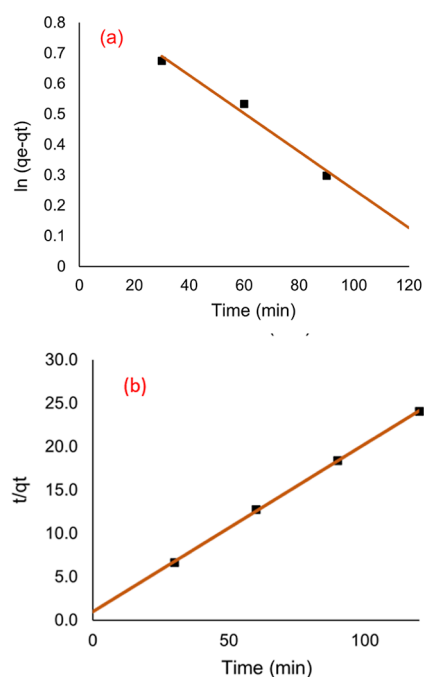
Figure 8. Fitted kinetics curves for CIP adsorption on Fe-POP by (a) pseudo-first-order model and (b) pseudo-second-order model.

Table 3. Kinetic Parameters and Error Values of the Pseudo-First-Order Model and the Pseudo-Second-Order Model

pseudo-first-order kinetic					
q_e	K_1	R^2	ERRSQ	HYBRID	ARE
2.40	0.006	0.980	10.963	19.645	14.276
pseudo-second-order kinetic					
q_e	K_2	R^2	ERRSQ	HYBRID	ARE
5.71	0.038	0.999	11.365	11.639	7.659

Systematic investigations were carried out to assess Fe-POP's adsorption potential in removing the antibiotic Ciprofloxacin (CIP) from aqueous solutions. Key parameters, such as adsorbent loading, pH, and antibiotic concentration, were varied to optimize the adsorption conditions. The impact of adsorbent loading was evaluated by introducing 12.5, 25, and 37.5 mg of Fe-POP to a 50 mL CIP solution (10 ppm). The adsorption capacity of CIP showed a slight increase from 114 to 121 mg g^{-1} with an increase in Fe-POP from 12.5 to 25 mg, but a further increase to 37.5 mg resulted in a decreased adsorption rate to 7.8 mg g^{-1} after 120 min. On the other hand, CIP adsorption was highest at pH 3, decreasing with an increase in pH at values of 7 and 11 due to the molecular interactions of CIP and Fe-POP. The impact of CIP concentration on the adsorption rate was explored at the optimal pH of 3, utilizing initial CIP concentrations of 5, 10, and 15 ppm in the presence of 25 mg of Fe-POP. The highest adsorption rate of CIP occurred at 5 ppm, reaching an adsorption capacity of 263 mg g^{-1}. However, an increase in the initial concentration of CIP from 5 to 15 ppm led to a reduction in the adsorption capacity to 155 mg g^{-1} after 180 min.

Under the optimal conditions at pH 3, CIP concentration of 5 ppm, and 25 mg Fe-POP, the maximum adsorption capacity reached an impressive 263 mg g^{-1}. Fitting the obtained data with the Langmuir adsorption isotherm ($R^2 = 0.962$) and the pseudo-second-order kinetic model ($R^2 = 0.999$), and error values, indicated that the adsorption process primarily relied on chemical interactions between CIP molecules and Fe-POP. Furthermore, the homogeneity of the Fe-POP surface was confirmed.

Therefore, Fe-POP demonstrated remarkable attributes, including a robust structure and a high adsorption capacity, making it highly effective in the removal of CIP contaminants from water. These findings underscore the potential of Fe-POP as a promising adsorbent for water treatment applications.

■ ASSOCIATED CONTENT

ⓈⒾ Supporting Information

The Supporting Information is available free of charge at https://pubs.acs.org/doi/10.1021/acsomega.3c09200.

Scheme and solid-state ^{13}C NMR spectrum of the synthesized Fe-POP (PDF)

■ AUTHOR INFORMATION

Corresponding Author

Masoumeh Taherimehr − *Department of Chemistry, Babol Noshirvani University of Technology, Babol 47148-71167, Iran;* ⓞ orcid.org/0000-0001-7354-4090; Email: m.taherimehr@nit.ac.ir

Authors

Shabnam Mehraban Khaledi − *Department of Chemistry, Babol Noshirvani University of Technology, Babol 47148-71167, Iran*

Seyed Karim Hassaninejad-Darzi − *Department of Chemistry, Babol Noshirvani University of Technology, Babol 47148-71167, Iran;* ⓞ orcid.org/0000-0002-9697-0874

Complete contact information is available at:

https://pubs.acs.org/10.1021/acsomega.3c09200

◼ REFERENCES

(1) Taherimehr, M.; Pescarmona, P. P. Green polycarbonates prepared by the copolymerization of CO2 with epoxides. *J. Appl. Polym. Sci.* **2014**, *131* (21), 41141.

(2) YousefniaPasha, H.; Mohtasebi, S. S.; Tabatabaeekoloor, R.; Taherimehr, M.; Javadi, A.; Soltani Firouz, M. Preparation and characterization of the plasticized polylactic acid films produced by the solvent-casting method for food packaging applications. *J. Food Process. Preserv.* **2021**, *45* (12), No. e16089.

(3) Gheytani, S.; Hassaninejad-Darzi, S.; Taherimehr, M. Formaldehyde Electro-catalytic Oxidation onto Carbon Paste Electrode Modified by MIL-101 (Cr) Nanoparticles. *Fuel Cells* **2020**, *20* (1), 3–16.

(4) Ansari Moghaddam, A.; Mohammadi, L.; Bazrafshan, E.; Batool, M.; Behnampour, M.; Baniasadi, M.; Mohammadi, L.; Nadeem Zafar, M. Antibiotics sequestration using metal nanoparticles: An updated systematic review and meta-analysis. *Inorg. Chim. Acta* **2023**, *550*, 121448.

(5) Nguyen, L. M.; Nguyen, N. T. T.; Nguyen, T. T. T.; Nguyen, T. T.; Nguyen, D. T. C.; Tran, T. V. Occurrence, toxicity and adsorptive removal of the chloramphenicol antibiotic in water: a review. *Environ. Chem. Lett.* **2022**, *20* (3), 1929–1963.

(6) Girardi, C.; Greve, J.; Lamshöft, M.; Fetzer, I.; Miltner, A.; Schäffer, A.; Kästner, M. Biodegradation of ciprofloxacin in water and soil and its effects on the microbial communities. *J. Hazard. Mater.* **2011**, *198*, 22–30.

(7) Ranjkesh, B.; Taherimehr, M. Application of mesoporous COK-15 metal-organic framework as medication carrier for acetaminophen and clindamycin. *Russ. J. Inorg. Chem.* **2021**, *66*, 68–77.

(8) Zhao, Z.; Lin, S.; Yu, Z.; Su, M.; Liang, B.; Liang, S.-X.; Ju, X.-H. Facile synthesis of triazine-based microporous organic network for high-efficient adsorption of flumequine and nadifloxacin: A comprehensive study on adsorption mechanisms and practical application potentials. *Chemosphere* **2023**, *315*, 137731.

(9) Zhu, B.; Song, D.; Jia, T.; Sun, W.; Wang, D.; Wang, L.; Guo, J.; Jin, L.; Zhang, L.; Tao, H. Effective visible light-driven photocatalytic degradation of ciprofloxacin over flower-like Fe3O4/Bi2WO6 composites. *ACS Omega* **2021**, *6* (2), 1647–1656.

(10) Gupta, A.; Garg, A. Degradation of ciprofloxacin using Fenton's oxidation: effect of operating parameters, identification of oxidized by-products and toxicity assessment. *Chemosphere* **2018**, *193*, 1181–1188.

(11) Alonso, J. J. S.; El Kori, N.; Melián-Martel, N.; Del Río-Gamero, B. Removal of ciprofloxacin from seawater by reverse osmosis. *J. Environ. Manage.* **2018**, *217*, 337–345.

(12) Javid, N.; Honarmandrad, Z.; Malakootian, M. Ciprofloxacin removal from aqueous solutions by ozonation with calcium peroxide. *Desalin. Water Treat.* **2020**, *174*, 178–185.

(13) Nasari, Z.; Taherimehr, M. Optimization of Visible-Light-Driven Ciprofloxacin Degradation Using a Z-Scheme Semiconductor MgFe2O4/UiO-67. *Langmuir* **2023**, *39* (40), 14357–14373.

(14) Wang, Y.; Shen, C.; Zhang, M.; Zhang, B.-T.; Yu, Y.-G. The electrochemical degradation of ciprofloxacin using a SnO2-Sb/Ti anode: influencing factors, reaction pathways and energy demand. *Chem. Eng. J.* **2016**, *296*, 79–89.

(15) Lu, D.; Xu, S.; Qiu, W.; Sun, Y.; Liu, X.; Yang, J.; Ma, J. Adsorption and desorption behaviors of antibiotic ciprofloxacin on functionalized spherical MCM-41 for water treatment. *J. Cleaner Prod.* **2020**, *264*, 121644.

(16) Movasaghi, Z.; Yan, B.; Niu, C. Adsorption of ciprofloxacin from water by pretreated oat hulls: Equilibrium, kinetic, and thermodynamic studies. *Ind. Crops Prod.* **2019**, *127*, 237–250.

(17) Verma, M.; Lee, I.; Sharma, S.; Kumar, R.; Kumar, V.; Kim, H. Simultaneous Removal of Heavy Metals and Ciprofloxacin Micropollutants from Wastewater Using Ethylenediaminetetraacetic Acid-Functionalized β-Cyclodextrin-Chitosan Adsorbent. *ACS Omega* **2021**, *6* (50), 34624–34634.

(18) Al-Musawi, T. J.; Mahvi, A. H.; Khatibi, A. D.; Balarak, D. Effective adsorption of ciprofloxacin antibiotic using powdered activated carbon magnetized by iron (III) oxide magnetic nanoparticles. *J. Porous Mater.* **2021**, *28*, 835–852.

(19) El-Kemary, M.; El-Shamy, H.; El-Mehasseb, I. Photocatalytic degradation of ciprofloxacin drug in water using ZnO nanoparticles. *J. Lumin.* **2010**, *130* (12), 2327–2331.

(20) Li, S.; Zhang, X.; Huang, Y. Zeolitic imidazolate framework-8 derived nanoporous carbon as an effective and recyclable adsorbent for removal of ciprofloxacin antibiotics from water. *J. Hazard. Mater.* **2017**, *321*, 711–719.

(21) Punyapalakul, P.; Sitthisorn, T. Removal of ciprofloxazin and carbamazepine by adsorption on functionalized mesoporous silicates. *Int. J. Environ. Eng.* **2010**, *4* (9), 412–416.

(22) Zhao, C.; Li, Y.; Chu, H.; Pan, X.; Ling, L.; Wang, P.; Fu, H.; Wang, C.-C.; Wang, Z. Construction of direct Z-scheme Bi5O7I/UiO-66-NH2 heterojunction photocatalysts for enhanced degradation of ciprofloxacin: Mechanism insight, pathway analysis and toxicity evaluation. *J. Hazard. Mater.* **2021**, *419*, 126466.

(23) Yang, Q.; Yu, H.; He, Y.; Liu, Z.; Qin, C.; Liu, B.; Li, Y. Porous three-component hybrid hydrogen-bonded covalent organic polymers: Design, synthesis and ciprofloxacin adsorption. *Eur. Polym. J.* **2020**, *123*, 109445.

(24) Saya, L.; Rameshwor Singh, W.; Hooda, S. Adsorptive removal of ciprofloxacin from aqueous medium by magnetic guar gum grafted graphene oxide nano composite. *J. Environ. Chem. Eng.* **2023**, *11* (5), 110766.

(25) Taheri, N.; Dinari, M.; Asgari, M. Recent applications of porous organic polymers prepared via Friedel-crafts reaction under the catalysis of AlCl3: a review. *ACS Appl. Polym. Mater.* **2022**, *4* (9), 6288–6302.

(26) Wang, W.; Zhou, M.; Yuan, D. Carbon dioxide capture in amorphous porous organic polymers. *J. Mater. Chem. A* **2017**, *5* (4), 1334–1347.

(27) Song, W.-C.; Xu, X.-K.; Chen, Q.; Zhuang, Z.-Z.; Bu, X.-H. Nitrogen-rich diaminotriazine-based porous organic polymers for small gas storage and selective uptake. *Polym. Chem.* **2013**, *4* (17), 4690–4696.

(28) Li, M.; Zhao, H.; Lu, Z.-Y. Porphyrin-based porous organic polymer, Py-POP, as a multifunctional platform for efficient selective adsorption and photocatalytic degradation of cationic dyes. *Microporous Mesoporous Mater.* **2020**, *292*, 109774.

(29) Zhang, Y.; Hong, X.; Cao, X.-M.; Huang, X.-Q.; Hu, B.; Ding, S.-Y.; Lin, H. Functional porous organic polymers with conjugated triaryl triazine as the core for superfast adsorption removal of organic dyes. *ACS Appl. Mater. Interfaces* **2021**, *13* (5), 6359–6366.

(30) Zhang, S.; Li, Y.; Shi, C.; Guo, F.; He, C.; Cao, Z.; Hu, J.; Cui, C.; Liu, H. Induced-fit adsorption of diol-based porous organic polymers for tetracycline removal. *Chemosphere* **2018**, *212*, 937–945.

(31) Wang, L.; Jin, P.; Duan, S.; She, H.; Huang, J.; Wang, Q. In-situ incorporation of Copper (II) porphyrin functionalized zirconium MOF and TiO2 for efficient photocatalytic CO2 reduction. *Sci. Bull.* **2019**, *64* (13), 926–933.

(32) Zhu, M.; Chen, J.; Huang, L.; Ye, R.; Xu, J.; Han, Y. F. Covalently grafting cobalt porphyrin onto carbon nanotubes for efficient CO2 electroreduction. *Angew. Chem., Int. Ed.* **2019**, *58* (20), 6595–6599.

(33) Patra, B. C.; Bhattacharya, S. New covalent organic square lattice based on porphyrin and tetraphenyl ethylene building blocks toward high-performance supercapacitive energy storage. *Chem. Mater.* **2021**, *33* (21), 8512–8523.

(34) Chen, Y.; Fang, Y.; Yu, J.; Gao, W.; Zhao, H.; Zhang, X. A silsesquioxane-porphyrin-based porous organic polymer as a highly

efficient and recyclable absorbent for wastewater treatment. *J. Hazard. Mater.* **2021**, *406*, 124769.

(35) Xiong, W.; Zeng, G.; Yang, Z.; Zhou, Y.; Zhang, C.; Cheng, M.; Liu, Y.; Hu, L.; Wan, J.; Zhou, C.; et al. Adsorption of tetracycline antibiotics from aqueous solutions on nanocomposite multi-walled carbon nanotube functionalized MIL-53 (Fe) as new adsorbent. *Sci. Total Environ.* **2018**, *627*, 235−244.

(36) Liu, J.; Zhou, B.; Zhang, H.; Ma, J.; Mu, B.; Zhang, W. A novel Biochar modified by Chitosan-Fe/S for tetracycline adsorption and studies on site energy distribution. *Bioresour. Technol.* **2019**, *294*, 122152.

(37) Jannat Abadi, M.; Nouri, S.; Zhiani, R.; Heydarzadeh, H.; Motavalizadehkakhky, A. Removal of tetracycline from aqueous solution using Fe-doped zeolite. *Int. J. Ind. Chem.* **2019**, *10* (4), 291−300.

(38) Zaher, A.; Taha, M.; Mahmoud, R. K. Possible adsorption mechanisms of the removal of tetracycline from water by La-doped Zn-Fe-layered double hydroxide. *J. Mol. Liq.* **2021**, *322*, 114546.

(39) Beiranvand, M.; Farhadi, S.; Mohammadi-Gholami, A. Adsorptive removal of tetracycline and ciprofloxacin drugs from water by using a magnetic rod-like hydroxyapatite and MIL-101 (Fe) metal-organic framework nanocomposite. *RSC Adv.* **2022**, *12* (53), 34438−34453.

(40) Alidadi, H.; Dolatabadi, M.; Davoudi, M.; Barjasteh-Askari, F.; Jamali-Behnam, F.; Hosseinzadeh, A. Enhanced removal of tetracycline using modified sawdust: Optimization, isotherm, kinetics, and regeneration studies. *Process Saf. Environ. Prot.* **2018**, *117*, 51−60.

(41) Modak, A.; Mondal, J.; Bhaumik, A. Porphyrin based porous organic polymer as bi-functional catalyst for selective oxidation and Knoevenagel condensation reactions. *Appl. Catal., A* **2013**, *459*, 41−51.

(42) Modak, A.; Nandi, M.; Mondal, J.; Bhaumik, A. Porphyrin based porous organic polymers: novel synthetic strategy and exceptionally high CO 2 adsorption capacity. *Chem. Commun.* **2012**, *48* (2), 248−250.

(43) Aniagor, C.; Abdel-Halim, E.; Hashem, A. Evaluation of the aqueous Fe (II) ion sorption capacity of functionalized microcrystalline cellulose. *J. Environ. Chem. Eng.* **2021**, *9* (4), 105703.

(44) Aniagor, C. O.; Sokker, H.; Hashem, A.; El-Hamaki, Y.; El-Degwi, M.; Abdel-Halim, E.; Hashem, A. Equilibrium studies on the uptake of nitrate and phosphate ions using functionalized carbon cloth. *J. Radioanal. Nucl. Chem.* **2021**, *329*, 1091−1102.

(45) Weber, J.; Schmidt, J.; Thomas, A.; Böhlmann, W. Micropore analysis of polymer networks by gas sorption and 129Xe NMR spectroscopy: toward a better understanding of intrinsic microporosity. *Langmuir* **2010**, *26* (19), 15650−15656.

(46) Sonwane, C.; Bhatia, S. Characterization of pore size distributions of mesoporous materials from adsorption isotherms. *J. Phys. Chem. B* **2000**, *104* (39), 9099−9110.

(47) Al-Maliky, E. A.; Gzar, H. A.; Al-Azawy, M. G. Determination of point of zero charge (PZC) of concrete particles adsorbents. *IOP Conf. Ser.: Mater. Sci. Eng.* **2021**, *1184*, 012004.

(48) Roca Jalil, M. E.; Baschini, M.; Sapag, K. Influence of pH and antibiotic solubility on the removal of ciprofloxacin from aqueous media using montmorillonite. *Appl. Clay Sci.* **2015**, *114*, 69−76.

(49) Luis Vázquez, J.; Berlanga, M.; Merino, S.; Domènech, Ò.; Viñas, M.; Teresa Montero, M.; Hernández-Borrell, J. Determination by Fluorimetric Titration of the Ionization Constants of Ciprofloxacin in Solution and in the Presence of Liposomes. *Photochem. Photobiol.* **2001**, *73* (1), 14−19.

(50) Gu, C.; Karthikeyan, K. Sorption of the antimicrobial ciprofloxacin to aluminum and iron hydrous oxides. *Environ. Sci. Technol.* **2005**, *39* (23), 9166−9173.

(51) Hamdaoui, O.; Naffrechoux, E. Modeling of adsorption isotherms of phenol and chlorophenols onto granular activated carbon: Part II. Models with more than two parameters. *J. Hazard. Mater.* **2007**, *147* (1−2), 401−411.

(52) Wei, F.; Wang, K.; Li, W.; Ren, Q.; Qin, L.; Yu, M.; Liang, Z.; Nie, M.; Wang, S. Preparation of Fe/Ni-MOFs for the Adsorption of Ciprofloxacin from Wastewater. *Molecules* **2023**, *28* (11), 4411.

(53) Abu Rumman, G.; Al-Musawi, T. J.; Sillanpaa, M.; Balarak, D. Adsorption performance of an amine-functionalized MCM-41 mesoporous silica nanoparticle system for ciprofloxacin removal. *Environ. Nanotechnol., Monit. Manage.* **2021**, *16*, 100536.

(54) Danalıoğlu, S. T.; Kerkez Kuyumcu, O.⸱⸱.; Abdel Salam, M.; Bayazit, Ş. S. Chitosan grafted SiO 2-Fe 3 O 4 nanoparticles for removal of antibiotics from water. *Environ. Sci. Pollut. Res.* **2018**, *25*, 36661−36670.

(55) Li, M.-f.; Liu, Y.-g.; Liu, S.-b.; Zeng, G.-m.; Hu, X.-j.; Tan, X.-f.; Jiang, L.-h.; Liu, N.; Wen, J.; Liu, X.-h. Performance of magnetic graphene oxide/diethylenetriaminepentaacetic acid nanocomposite for the tetracycline and ciprofloxacin adsorption in single and binary systems. *J. Colloid Interface Sci.* **2018**, *521*, 150−159.

(56) Shikuku, V. O.; Mishra, T. Adsorption isotherm modeling for methylene blue removal onto magnetic kaolinite clay: a comparison of two-parameter isotherms. *Appl. Water Sci.* **2021**, *11* (6), 103.

(57) Ebelegi, A. N.; Ayawei, N.; Wankasi, D. Interpretation of adsorption thermodynamics and kinetics. *Open J. Phys. Chem.* **2020**, *10* (03), 166−182.

(58) Mashhadimoslem, H.; Safarzadeh Khosrowshahi, M.; Jafari, M.; Ghaemi, A.; Maleki, A. Adsorption equilibrium, thermodynamic, and kinetic study of O2/N2/CO2 on functionalized granular activated carbon. *ACS Omega* **2022**, *7* (22), 18409−18426.